Ionomer Optimization for Water Uptake and Swelling in Anion Exchange Membrane Electrolyzer: Hydrogen Evolution Electrode

Garrett Huang[1], Mrinmay Mandal[1], Noor Ul Hassan[2], Katelyn Groenhout[1], Alexandra Dobbs[1], William E. Mustain[2], and Paul A. Kohl[1,*]

[1]School of Chemical and Biomolecular Engineering, Georgia Institute of Technology, Atlanta, Georgia, USA

[2]Department of Chemical Engineering, University of South Carolina, Columbia, South Carolina, USA

Keywords: anion conductive ionomer (ACI), anion exchange membrane (AEM), vinyl addition, poly(norbornene), cross-linking, water electrolysis, hydrogen

*Contact author: kohl@gatech.edu, 404-894-2893

Abstract

Green hydrogen produced through anion exchange membrane water electrolysis is a promising, low-cost chemical storage solution for intermittent renewable energy sources. Low-temperature electrolysis using anion exchange membranes (AEM) combines the benefits of established water electrolysis technologies based on alkaline electrolysis and proton exchange membrane electrolysis. The anion conductive ionomers (ACI) used in the AEM electrolyzer (AEMEL) electrodes has been investigated. The ACI serves two primary purposes: (i) facilitate hydroxide conduction between the catalyst and bulk electrolyte and (ii) bind the catalyst to the porous transport layer and membrane. High ion exchange capacity (IEC) ACIs are desired, however, high IEC can cause excessive water uptake (WU) and detrimental ACI swelling. Proper water management is a key factor in obtaining maximum performance in AEM-based devices. In this study, a series of poly(norbornene)-based ACIs were synthesized and deployed in hydrogen evolving AEMEL cathode electrodes. A balance between ionic conductivity, WU and ionomer swelling was achieved in the ACI by varying the IEC and degree of polymer cross-linking. It was found that higher IEC ACIs with light crosslinking are preferred in the HER electrode. Such a configuration fine-tuned the WU and ionomer swelling to achieve optimum cell performance and reduce cell operating voltages.

Introduction

Renewable energy from wind and solar can be used to supply significant global energy.[1] However, renewable technologies are intermittent and require a reliable and economical way of storing energy. Hydrogen produced via water electrolysis is a promising method for on-site chemical energy storage or local generation of hydrogen at the point-of-use. Green hydrogen can be transported and used on-demand in fuel cell-powered applications for transportation or base-load power.

Anion exchange membrane electrolyzers (AEMEL) are a low-cost alternative to existing commercially available low-temperature electrolysis technologies such as liquid-electrolyte alkaline electrolyzers (AEL) or proton exchange membrane electrolyzers (PEMEL).[2] AEMELs can theoretically combine the advantages of AELs and PEMELs. The alkaline environment enables more facile oxygen evolution reaction (OER) kinetics and the use of non-platinum group metal (PGM) electrocatalysts.[1-11] The inexpensive solid polymer electrolyte design lowers the overall cost by eliminating the need for electrolyte recirculation and allows for a compact system design that can directly deliver high-purity, pressurized hydrogen.[1, 12-18]

In an AEMEL, hydroxide ions are oxidized at the positive electrode (i.e., anode) producing oxygen and water, as shown in Figure 1. At the negative electrode (i.e., cathode), water is reduced to form hydrogen and hydroxide ions. In many AEMELs, including those of commercial interest, liquid water is fed to the oxygen-evolving positive electrode and not the negative electrode so that the hydrogen gas is less humid and can more easily be compressed without having to separate it from liquid water.[17, 19] Thus, the water feed to the AEMEL cathode is by back diffusion of water from the anode to the cathode through the AEM. The activity of water at the electrode surface is influenced by the rate of water diffusion through the membrane and hydrophilicity of the anion

conductive ionomers (ACIs). Excess water in the cathode can lead to electrode flooding and a high cathode overpotential. Inadequate water content can result in electrode dry-out which may limit the rate of hydrogen production and degrade the electrode materials because the pH is too high.

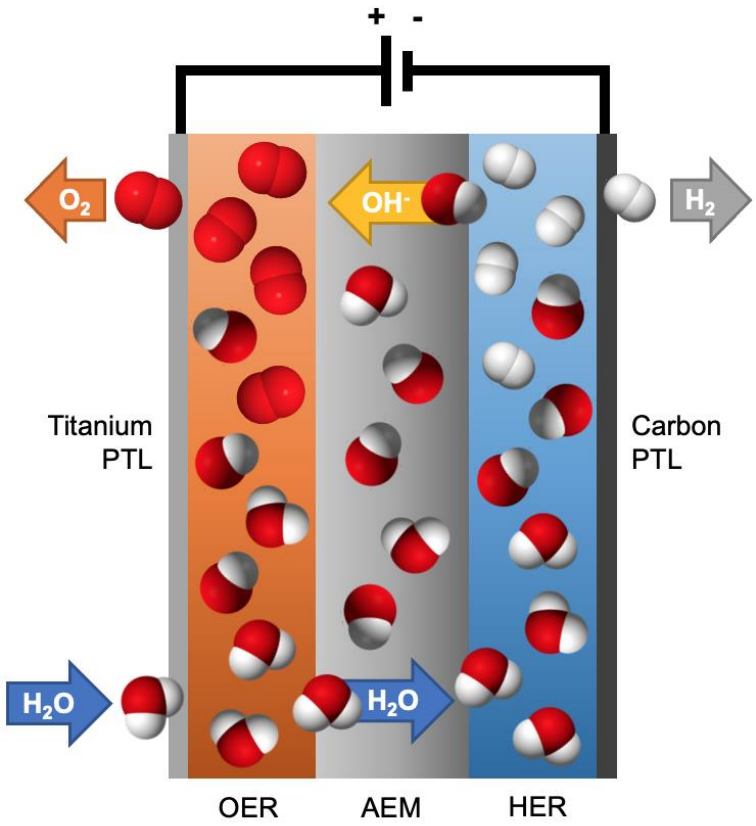

$$Anode: 4OH^- \rightarrow O_2 + 2H_2O + 4e^- \quad E_0 = 0.401\,V$$

$$Cathode: 4H_2O + 4e^- \rightarrow 2H_2 + 4OH^- \quad E_0 = -0.828\,V$$

$$Overall: 2H_2O \rightarrow 2H_2 + O_2 \quad E_0 = 1.23\,V$$

Figure 1. Diagram of the low-temperature AEM electrolysis cell configuration and associated half-reactions.

The anion exchange membrane (AEM) based systems have become competitive with their proton exchange membrane counterparts. High conductivity (>200 mS/cm), stable, low-cost AEMs have been developed in recent years. They have been successfully deployed in

hydrogen/oxygen AEM fuel cells, with some being able to achieve up to 3.5 W/cm^2 peak power density.[20-28] The properties of such high-performing membranes are also attractive to AEMELs. AEM fuel cell work has also shown that the properties of the ACI can play a significant role in the device performance[28], however, the ACI in the catalyst layers of AEM electrolyzers has received little attention.[14, 29]

The primary purpose of the ionomer in the AEMEL electrodes is to provide an ionic pathway between the catalyst sites and AEM. High ionic conductivity and chemical stability are desired in electrolyzer ionomers, however, mechanical strength is not as important in the ACI compared to the AEM because the ACI does not form a free-standing layer.[30-32] The second purpose of the ionomer is to provide adhesion of the catalyst layer within the electrode to the porous current collector and membrane. Good adhesion is critical in the electrolyzer cathode where hydrogen gas is formed. Gas formation may cause delamination of the electrode from the membrane or detach the catalyst from the electrode.[33] Third, the ACI must facilitate water transport between the catalyst and the AEM, and be able to do so while avoiding excessive water uptake (WU). Excessive ionomer swelling can disrupt the three-phase boundary between the catalyst, ionomer and porous transport layer and choke-off the ionic or electronic pathway to the catalyst sites.[24, 34-39] It can also reduce the rate of gas bubble removal which would decrease performance by limiting the pore volume available for mass transport within the electrodes.

In a previous report, the ACI in the oxygen evolution electrode (OER) was optimized through a trade-off between conductivity and WU.[29] In this study, a family of poly(norbornene) tetrablock copolymers were synthesized and used to investigate the properties of the hydrogen evolution reaction (HER) ionomer in low-temperature AEM electrolysis cells. The ion exchange capacity (IEC) of the ionomers (1.49 to 3.60 meq/g) was adjusted by controlling the ratio of ion

conducting to non-ion conducting norbornene monomers in the ACI and used to control the hydrophilicity and water uptake within the cathode catalyst layer. Ionic conductivity and swelling due to WU are especially important at the negative electrode because water is used as a reactant in the HER. Light cross-linking of the ionomer was used to maintain adequate WU in high IEC ionomers without the penalty of excessive swelling or dry-out. Optimization of the ionomer loading was also performed. This work compliments a previous study regarding the use of cross-linked high IEC OER ionomer in an AEM water electrolyzer and highlights for the first time the differences in ionomer requirements between the OER and HER electrodes.

Experimental

Synthesis: Poly(norbornene) (PNB) tetrablock copolymers were used for both the AEMs and ACIs in this study. The polymers were synthesized and characterized by the method previously reported by Mandal et al, Scheme 1.[20] Briefly, the tetrablock copolymer was synthesized in a vinyl-addition polymerization reaction. A bromoalkyl tether was used in the cross-linking reaction. Non-cross-linked bromoalkyl tethers were aminated using trimethyl amine (TMA) followed by ion exchange of the bromide ions for hydroxide ions.

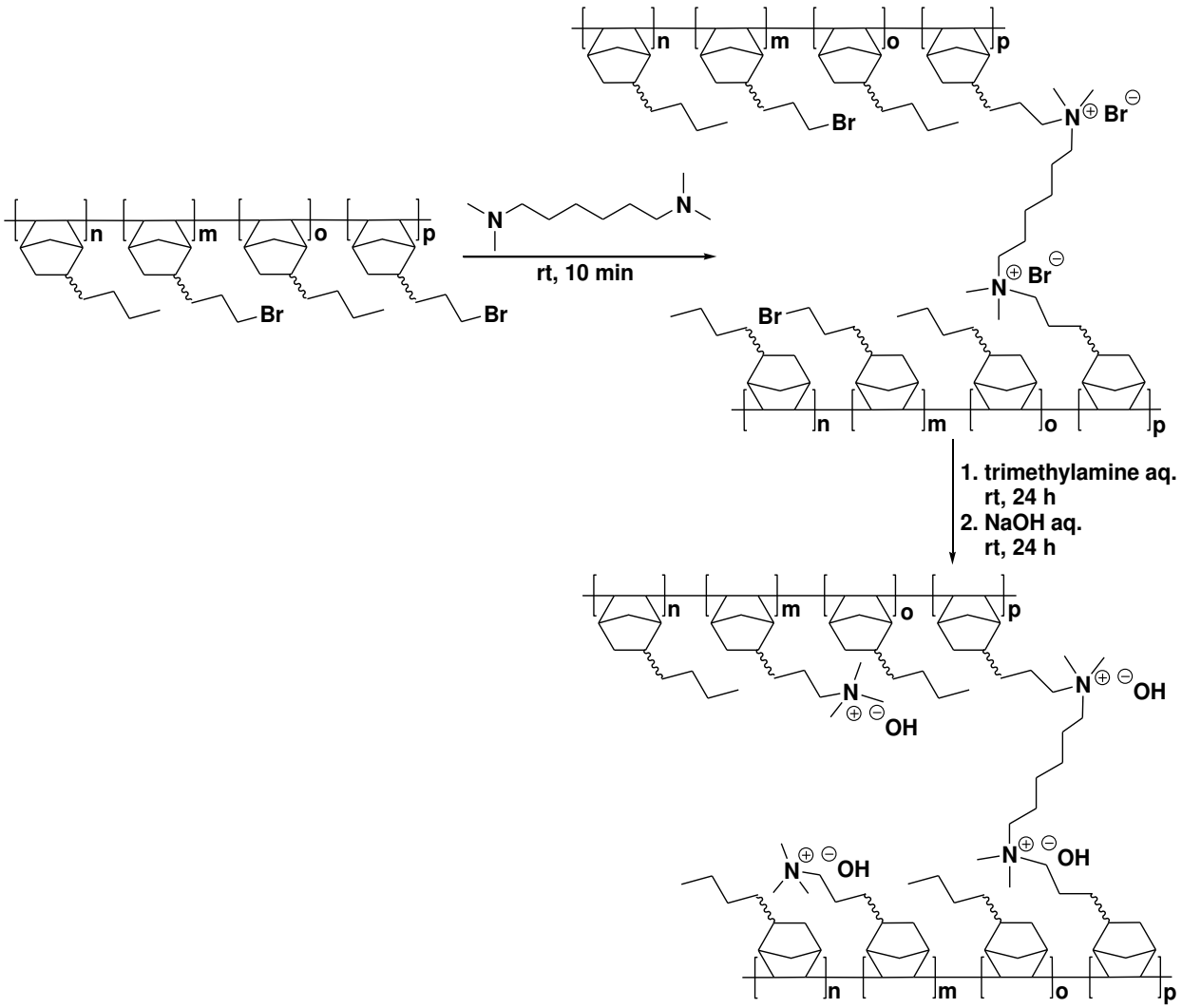

Scheme 1. Synthesis and cross-linking of poly(norbornene) ACI.

The IEC of the ionomer was controlled by tuning the ratio of hydrophobic butyl norbornene (BuNB) and hydrophilic bromoalkyl norbornene (bromopropyl norbornene (BPNB) or bromobutyl norbornene (BBNB)) blocks. No obvious difference was found between the bromopropyl and bromobutyl forms of the polymers in synthesis or performance. IEC was calculated based on ^{1}H NMR analysis using a Bruker Avance 400 MHz NMR instrument using $CDCl_3$ as the solvent.[40] The number average molecular weight (M_n) and dispersity index (Đ) of the polymers were measured by gel permeation chromatography (GPC) on a Shimadzu GPC

(DGU-20A, LC-20AD, CTO-20A, and RID-20A), a Shodex column (KF-804L), with HPLC grade THF (1 mL/min flow rate at 30 °C) eluent and calibrated against a polystyrene standard as previously described.[20-22] IEC, molecular weight and dispersity index were measured with the ionomer in bromoalkyl form. The ionomers were soaked in 50 wt% aqueous trimethylamine (TMA) solution at room temperature for 48 h to convert the bromoalkyl blocks into quaternary ammonium head-groups.

Ionomers: Poly(norbornene) ACIs were made by first solvent casting the polymer/toluene solution into films. Ionomers with light cross-linking were made by adding 1, 3, 5 or 10 mol% of a cross-linking agent, N,N,N',N'-tetramethyl-1,6-hexanediamine (TMHDA), with respect to the number of available bromoalkyl sites in the polymer. The solution consisting of polymer and cross-linker was solvent cast into a shallow aluminum dish and allowed to dry overnight in a tube furnace. The polymer was then soaked in 50 wt% aqueous TMA solution at room temperature for 48 h to convert the remaining uncross-linked bromoalkyl sites to quaternary ammonium head-groups. The remaining solvent was evaporated in a vacuum oven (0.5 atm) at 60 °C after thoroughly washing with DI water. The dried, quaternized ACI was milled into fine powder using a high-speed grinder with dry ice. The in-plane conductivity was measured using a 4-point probe with the membrane submerged in HPLC grade water after conversion to the hydroxide form. The WU of the ionomer samples was measured by soaking the material in liquid water and subtracting the dry polymer mass from the hydrated polymer mass. The hydrated material was dried in a vacuum oven (0.5 atm) for 48 h at 60 °C prior to measurement. The WU is expressed in terms of percent water per mass of dry polymer.

Membranes: The AEMs used in this study were formed by casting the tetrablock copolymer into a film with a proprietary polymer reinforcement (Pention®, Xergy Inc.). 5, 10 or

15 mol% TMHDA cross-linker was used relative to the mol% of the halogenated monomers in the polymer. Unreinforced membranes cast using GT74 tetrablock copolymer (74 mol% BBNB, IEC = 3.60 meq/g, *Mn* = 40.35 kDa, Đ = 1.26) with 5 mol% cross-linking were used in some experiments. The thickness of the AEMs is specified in the experiments described in the Results section.

Electrodes and Membrane Electrode Assembly: Anodes and cathodes were fabricated using the catalyst-coated substrate (CCS) method by using an airbrush to spray catalyst ink directly onto the porous transport layer (PTL). The dry ACI powder was first ground into fine particles using a mortar and pestle. The loading (wt%) of the ACI is specified in the experiments described in the Results section. The ACI was wetted with a small amount of DI water (1mL) and allowed to sit for 20 to 30 min before use. The hydrated ionomer was then wet-ground for 10 min using a mortar and pestle. 200 mg of platinum supported on carbon black (Pt/C, Nel Hydrogen) or 30 wt% platinum-nickel alloy on ECS-3701 (PtNi, Pajarito Powder) was added to the ACI and mixed together with the mortar and pestle to form the cathode catalyst ink. 5 mL of isopropyl alcohol (IPA) was added to the solid mixture and ground for an additional 10 min to break-up any aggregates. The mixture was then completely transferred to a vial and another 9 mL of IPA was added to create the catalyst ink. The ink was sonicated for at least 60 min in an ice bath before it was hand sprayed with an airbrush onto the PTL (Toray TGP-H-090 with 5% wetproofing) to produce a 16 cm^2 electrode.

The same fabrication method was used for the anode using iridium oxide (IrO_2, Nel Hydrogen) or lead ruthenate ($PbRuO_x$, Pajarito Powder) to form the catalyst ink. In the anode, the ionomer loading was held constant (25 wt%) and the ink was sprayed onto platinized titanium

PTLs from Nel Hydrogen. The target catalyst loading of the cathode and anode electrodes were both 2 mg/cm^2.

The membrane electrode assemblies (MEAs) were made by cutting electrodes (4 cm^2) from the larger, 16 cm^2 anode and cathode sheets. The AEM (5 cm^2), cathode and anode were individually ion exchanged to the OH^- form by soaking in 1.5 M NaOH solution for a total of 60 min refreshing the base solution every 20 minutes prior to cell assembly. A nitrogen cover gas was applied during the entire ion exchange to avoid carbonation from atmospheric CO_2. The AEM was placed between the two electrodes and pressed together in the 5 cm^2 Fuel Cell Technologies hardware between two 316 stainless steel single-pass serpentine flow-fields and 10 mil Tefzel gaskets. The torque applied to the cell hardware was 25 in-lb.

Electrolyzer Testing: The MEAs were tested using a custom-built electrolysis test station and operated at a cell temperature of 50 °C. Potassium carbonate in DI water (1 wt%) was supplied at 0.2 L/min to the anode side. The cathode side was at atmospheric pressure. The cell was allowed to equilibrate at the desired temperature for 1 hr before testing. A linear polarization sweep was performed prior to break-in of the cell. Cell break-in was performed by first applying 125 mA/cm^2 current until the cell voltage no longer changed. The current density was then increased and allowed reach steady-state in steps of 250 mA/cm^2 until the desired operating current density was reached. Additional polarization curves were taken periodically throughout the course of the operational test. The high frequency resistance (HFR) of the cell was measured via electrochemical impedance spectroscopy (EIS) using a Metrohm Autolab B.V. Type PGSTAT204 potentiostat. Measurements were conducted at 0.01 A with a frequency range from 10 kHz to 0.1 Hz. The area specific resistance (ASR) was calculated from the EIS data.

Results

A representative NMR spectrum of the synthesized polymer is shown in Figure 2, which shows distinct peaks for both bromopropyl norbornene and butyl norbornene monomers. The peaks at 0.89 ppm and 3.41 ppm correspond to terminal methyl protons (H_a) of the butyl norbornene block and methylene protons (H_b) of the bromopropyl norbornene block, respectively. The integration ratio of H_a and H_b was used to calculate the IEC and mol% of the halogenated block.[20, 21]

The physical properties of the poly(norbornene) tetrablock copolymer ACI ionomers are given in

Table *1*. In Table 1, the ionomers are denoted as GTXX, where XX is the mol% of bromoalkyl norbornene monomer (resulting in the quaternary ammonium head group) in the block copolymer. Larger XX values result in a higher IEC and WU. Ionomers were prepared with IEC values ranging from 1.49 to 3.60 meq/g. Non-crosslinked version of GT69, GT72 and GT74 ionomers were soft and swollen when hydrated and their WU was greater than 1000%. Therefore, 5 mol% TMHDA crosslinker was added to these ACIs to control WU and swelling. Free-standing films of the cross-linked polymers were mechanically robust and could easily be handled.

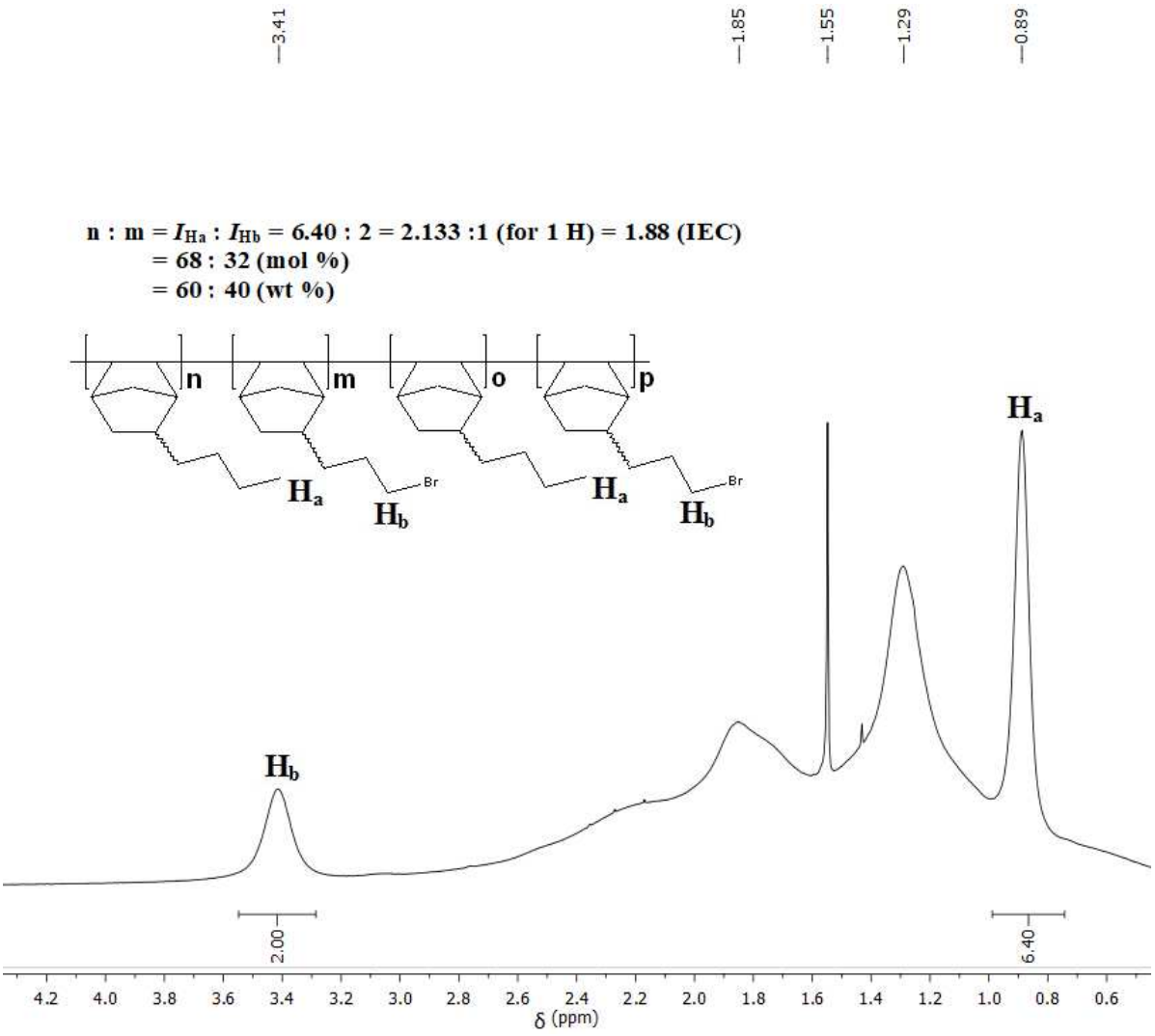

Figure 2. Representative NMR spectrum of GT32 ionomer.

The hydroxide conductivity of the ionomer samples also increased with IEC. The conductivity of all samples doubled when the temperature was increased from 25 °C to 80 °C. The dispersity index of all the ionomer samples was similar and ranged from 1.17 to 1.88, averaging 1.47. The number average molecular weight (M_n) of the ionomer samples ranged from 40.4 to

116.4 kDa. A representative GPC trace of GT32 ionomer is shown in Figure 3. The ratio σ/IEC, in units of g S/cm eq, is a measure of ion mobility in the polymer and is reported in

Table *1*. The mobility tended to track with molecular weight in the polymer films. For example, GT32 and GT69 had the highest molecular weight and mobility.

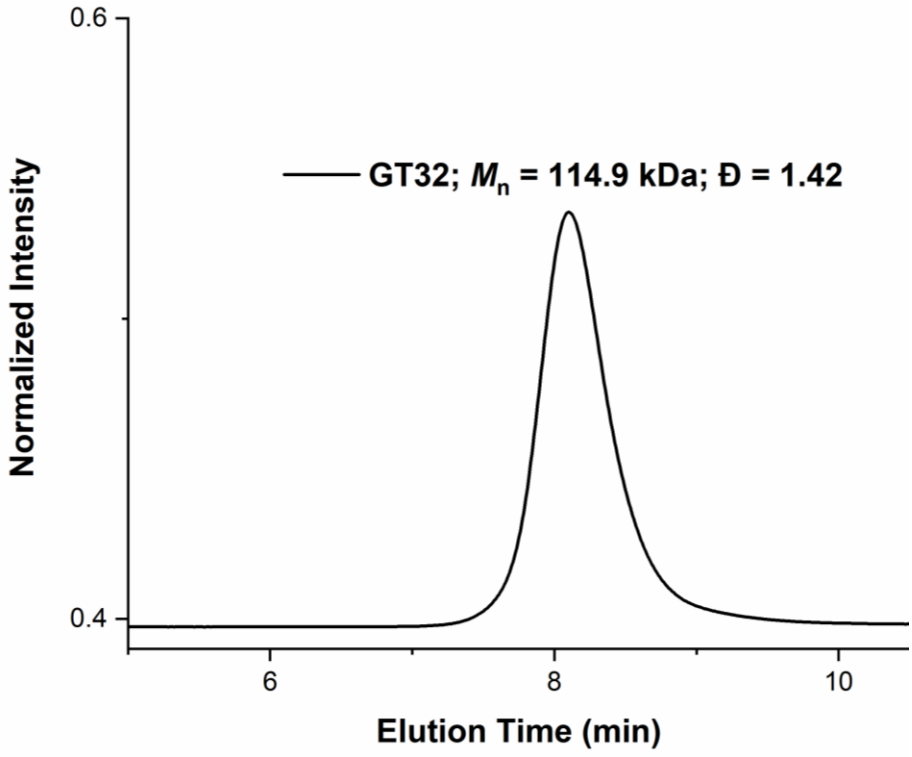

Figure 3. Representative GPC trace of GT32 ionomer

Table 1. Properties of poly(norbornene) ionomers.

Sample	***Mn*** **(kDa)**	**Đ**	**IEC (meq/g)**	**Ionic Conductivity (mS/cm)**		**σ/IEC (g S/cm eq) (80 °C)**	**WU (%)**
				25 °C	**80 °C**		
GT25	68.6	1.88	1.49	27.5	60.4	40.5	24
GT32	114.9	1.42	1.88	62	123	65.4	63

GT38	50.8	1.54	2.21	51	102	46.2	71
GT69 [a]	116.4	1.56	3.38	89	178	52.7	115
GT72[a]	68.2	1.17	3.50	83	175	50.0	96
GT74[a]	40.4	1.26	3.56	80	160	44.9	103

[a] σ and WU measured with 5 mol% TMHDA cross-linker. GT38 and GT32 were synthesized using BPNB as the halogenated block and the others used BBNB. IEC was determined by ^{1}H NMR in bromide form. Standard deviation for WU was ± 3%. ND = not determined.

After determining their physical properties, the ACIs were integrated into AEMEL cathode electrodes and their electrolyzer performance was characterized. The ACI content in the hydrogen-evolving cathode was first investigated by comparing MEAs with four GT74 ionomer loadings: 10%, 15%, 20% and 30%. The tests were performed at 1 A/cm^2 and identical anodes. The resulting cell voltage using the four ACIs was 1.80 V, 1.82 V, 1.82 V and 1.86 V for the MEAs with 10%, 15%, 20% and 30% HER ionomer content, respectively. The area specific resistances of the four MEAs were similar, though there was a slight increase with ionomer content: 0.83 Ω-cm^2 (10% ionomer), 0.84 Ω-cm^2 (15% ionomer), 0.86 Ω-cm^2 (20% ionomer) and 0.87 Ω-cm^2 (30% ionomer). Figure 4 shows a comparison of the polarization curves of the MEAs with the different ionomer content in the HER catalyst layer. Figure 5 shows the steady state response for these MEAs operated at 1 A/cm^2. This set of results shows that the electrode with 10% ionomer gave the best performance, although there was not a sharp drop-off from 10% to 20% ionomer. Electrodes with less than 10% ionomer content did not perform as well. It is also noted that higher ionomer content (i.e., 30% in Figure 5) showed an increase in current with time indicative of electrode flooding.

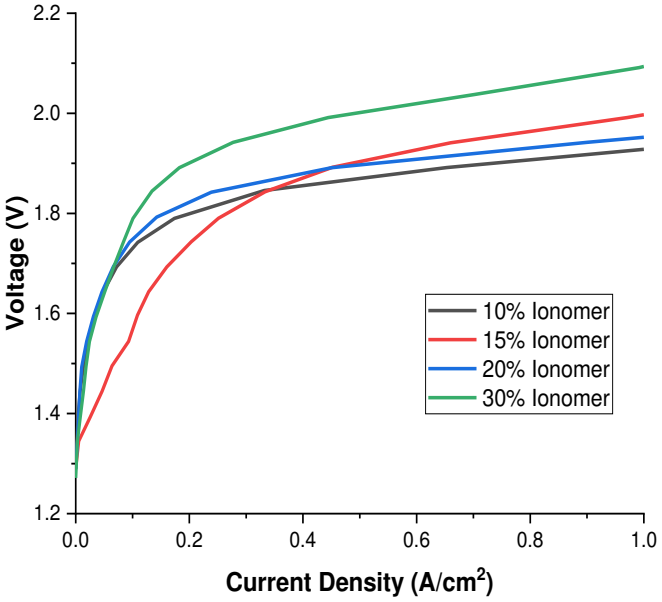

Figure 4. Comparison of polarization curves of MEAs with various HER ionomer content. The AEM was GT69 with a PTFE reinforcement (40 μm thick, 15 mol% cross-linking). The anode ionomer was GT25 (25 wt%) and catalyst was $PbRuO_x$. The cathode ionomer was GT74 and the catalyst was PtNi.

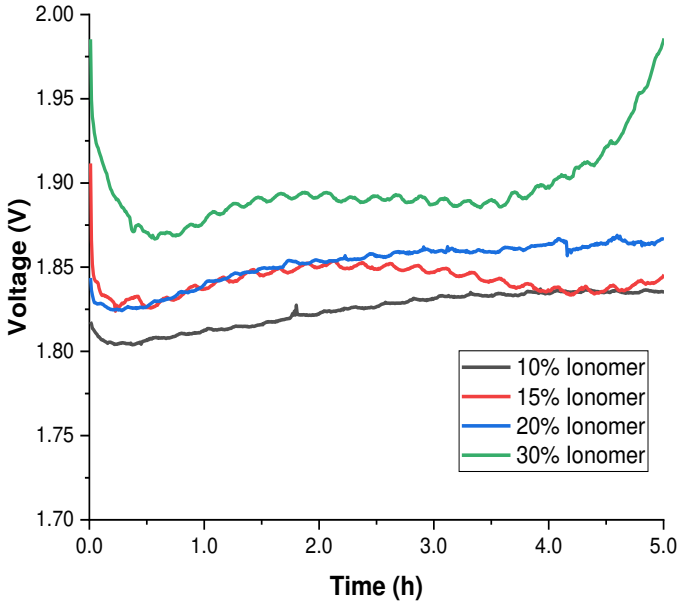

Figure 5. Cell voltage vs. time for MEAs with various HER ionomer content at 1 A/cm^2. The AEM was GT69 with a PTFE reinforcement (40 μm thick, 15 mol% cross-linking). The anode ionomer

was GT25 (25 wt%) and catalyst was $PbRuO_x$. The cathode ionomer was GT74 and catalyst was PtNi.

Next, the effect of HER ionomer IEC was investigated at a constant ionomer loading of 20 wt%. Figure 6 shows polarization curves from 0 to 500 mA/cm^2 for AEMELs with cathode ionomers with relative low IEC (GT32) and high IEC (GT74). From the polarization curve, both MEAs performed similarly at low current density (100 mA/cm^2). At 100 mA/cm^2, where the reaction kinetics dominate, the two MEAs had very similar cell voltage, 1.68 V and 1.67 V for cathodes containing GT32 and GT74, respectively. However, at a higher current density of 500 mA/cm^2, the cell voltage of the MEA with GT74 in the cathode was 100 mV lower than the MEA with GT32 in the cathode (2.11 V vs. 2.21 V). Fi 7 shows the cell voltage vs. time for these two MEAs at 500 mA/cm^2 constant-current operation. The electrode with GT74 trended toward lower cell voltage with time, down to 2.05 V while GT32 trended up to 2.26 V. The upward trend of GT32 with time may be indicative of electrode dry out as the electrode consumes water. These trends indicate that water balance in the HER electrode is a critical factor with dry-out possible with GT32 (i.e., rising voltage with time) and GT74 showing adequate water retention to support 500 mA/cm^2.

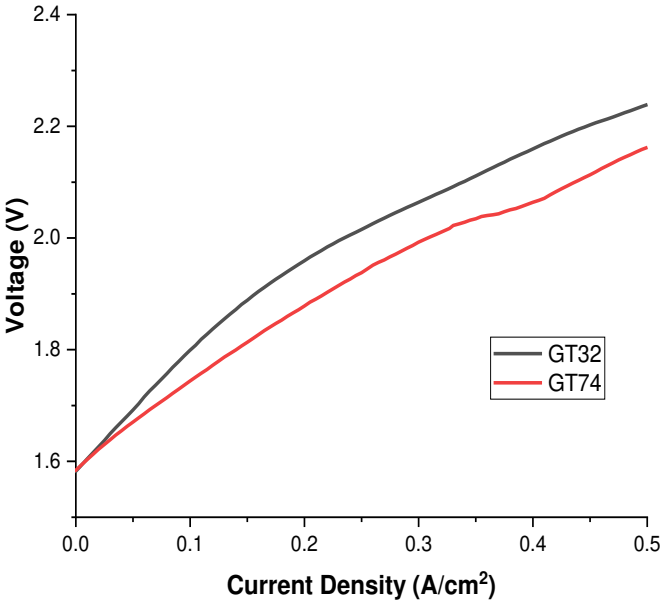

Figure 6. Comparison of polarization curves of MEAs with HER ionomers of high and low ion exchange capacities. The AEM was unreinforced GT74 (54 μm thick, 5 mol% cross-linking). The cathode catalyst was Pt/C. The anode ionomer was GT38 (25 wt%) and the catalyst was IrO_2.

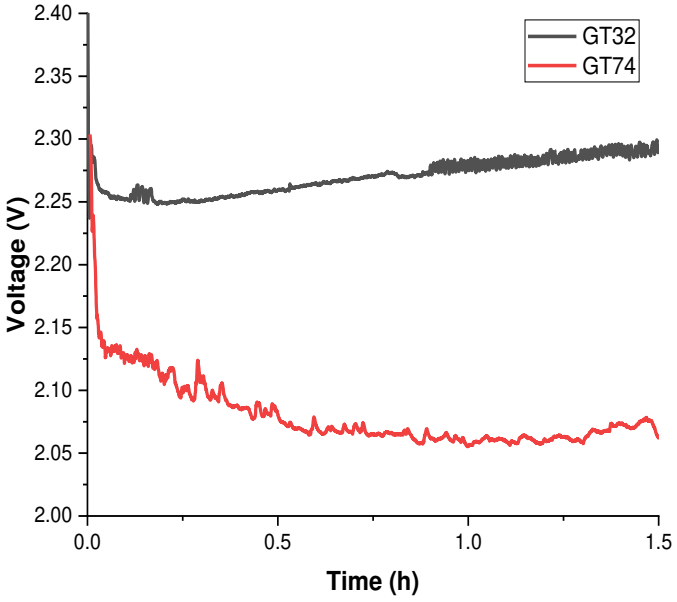

Figure 7. Cell voltage vs. time for MEAs with high and low IEC HER ionomers at 500 mA/cm^2. The AEM was unreinforced GT74 (54 μm thick, 5 mol% cross-linking). The cathode catalyst was Pt/C. The anode ionomer was GT38 (25 wt%) and the catalyst was IrO_2.

The effect of ionomer WU in the HER electrode was investigated by controlling the swelling in the ACI polymer through polymer cross-linking. Cross-linked, high IEC ionomers were used because they have high ionic conductivity and high WU which is the established HER preference (above). A high IEC tetrablock copolymer, GT72 (IEC = 3.54 meq/g, M_n = 68.2 kDa), was selected as the baseline polymer for the cross-linked HER ACI experiments. Four levels of cross-linking (1 mol%, 3 mol%, 5 mol% and 10 mol%) were used and are denoted as GT72-Y, where Y represents the mol% of cross-linker relative to the available cationic sites within the ionomer. The physical and electrochemical properties of the cross-linked ionomers were measured and are listed in Table 2. The hydroxide conductivity of GT72, GT72-1 and GT72-3 could not be measured because there was insufficient cross-linker to form a mechanically stable, free-standing film for measurement, although the polymers could be used as ionomer. GT72 had a high degree of swelling without any cross-linking and the estimated WU was greater than 1000%. The WU decreased significantly with increasing cross-linker content. The WU of GT72-1 was less than half that of the uncross-linked version (502%). Further increases in the cross-linker content lowered the WU to 198% (GT72-3), 96% (GT72-5) and 78% (GT72-10). The IEC of the cross-linked samples not significantly affected by cross-linker content, ranging from 3.47 (GT72-10) to 3.54 meq/g (GT72). The conductivity of the cross-linked ionomers remained high (>150 mS/cm) but decreased slightly with cross-linker content.

Figure 8 shows the polarization curves for AEMELs deploying the cross-linked ionomers from 0 to 500 mA/cm^2. At low current density (100 mA/cm^2), the performance of all of the MEAs was nearly identical. The difference in performance was more distinguishable at high current density (500 mA/cm^2). The trend observed at 1 A/cm^2, Figure 9, matched the trend in the polarization curves. The MEA with 10 mol% cross-linker had the highest steady-state cell voltage

among all samples tested (1.89 V). The MEA with 5 mol%, and 1 mol% cross-linker had cell voltages of 1.84 V and 1.80 V, respectively. The MEA with no cross-linker had a cell voltage of 1.83 V. The MEA with 3 mol% cross-linker had the best constant-current cell voltage among all samples tested, 1.77 V, which was an improvement of 120 mV over the MEA with 10 mol% crosslinker. The constant-current cell voltage (at 1 A/cm^2) and water uptake as a function of the amount of cross-linker are plotted in Figure 10. A minimum in-cell voltage at 3 mol% cross-linker was observed with a corresponding water uptake of 198%.

The effect of ACI molecular weight was tested by comparing the performance of the GT72 ionomers with GT74, a low molecular weight ionomer with similar IEC. GT74 had a number average molecular weight of 40.4 kDa, IEC of 3.60 meq/g and WU of >1000%. In comparison, GT72 had a number average molecular weight of 68.2 kDa, IEC of 3.54 meq/g and WU of >1000%. The performance of a cross-linked version of the lower molecular weight ionomer, GT74-3, with 3% TMHDA was also compared with GT72-3. GT74-3 and GT72-3 had similar IEC (3.58 vs. 3.52 meq/g) and WU (219% vs. 198%). Figure 11 shows the cell voltage vs. time at 1 A/cm^2 for the MEAs fabricated with high and low molecular weight ACI at the same cross-linker concentration. The cell voltage of the MEA with GT74 was 1.82 V, which was similar in performance to the MEA with GT72 (1.83 V). The addition of cross-linker to GT74 showed an 18 mV increase in cell voltage compared to its non-cross-linked form.

Table 2. Properties of cross-linked ionomers.

Sample	**Cross-linking (mol%)**	**IEC (meq/g)**	**Ionic Conductivity (mS/cm)**		**σ/IEC (g S/cm eq) (80 °C)**	**WU (%)**
			25 °C	**80 °C**		
GT72	0	3.54	ND	ND	ND	>1000
GT72-1	1	3.53	ND	ND	ND	502
GT72-3	3	3.52	ND	ND	ND	198
GT72-5	5	3.50	83	175	50.0	96
GT72-10	10	3.47	69	153	44.1	78
GT74	0	3.60	ND	ND	ND	>1000
GT74-3	3	3.58	ND	ND	ND	219

IEC was determined by ^{1}H NMR in bromide form. Standard deviation for WU was ± 3%. ND = not determined.

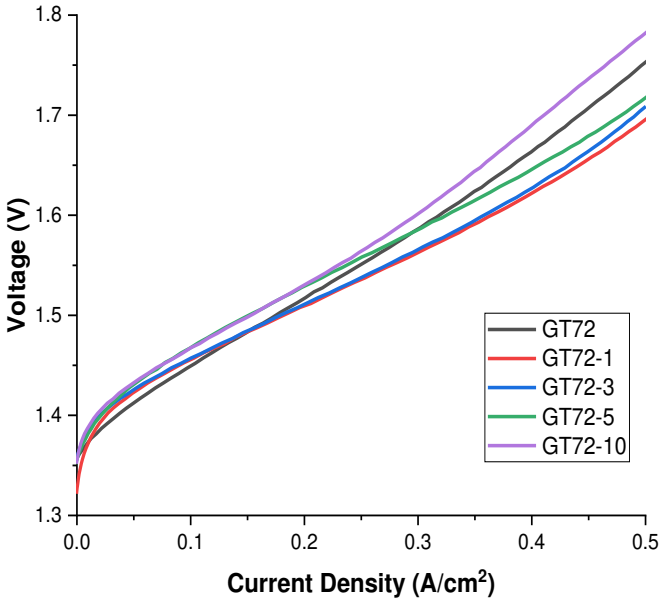

Figure 8. Comparison of polarization curves of MEAs with cross-linked HER ionomers. The AEM was GT72 with PTFE reinforcement (30 μm thick, 10 mol% cross-linking). The anode ionomer was GT72-10 (25 wt%) and catalyst was $PbRuO_x$. The cathode catalyst was PtNi.

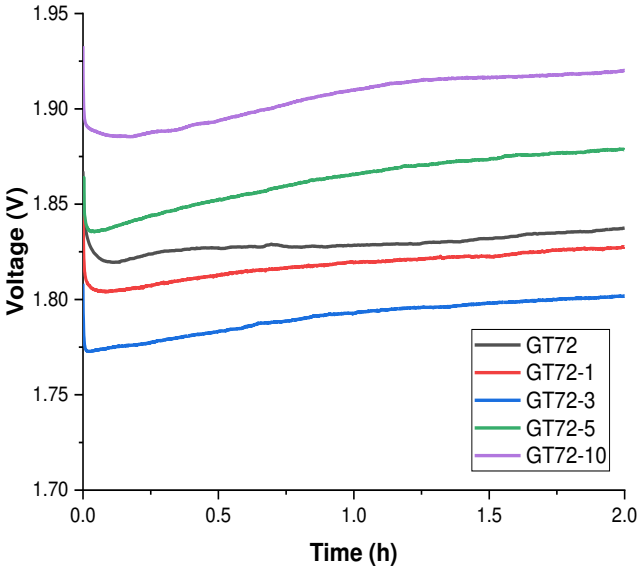

Figure 9. Cell voltage vs. time for MEAs with cross-linked, high IEC HER ionomers at 1 A/cm^2. The AEM was GT72 with PTFE reinforcement (30 μm thick, 10 mol% cross-linking). The anode ionomer was GT72-10 (25 wt%) and catalyst was $PbRuO_x$. The cathode catalyst was PtNi.

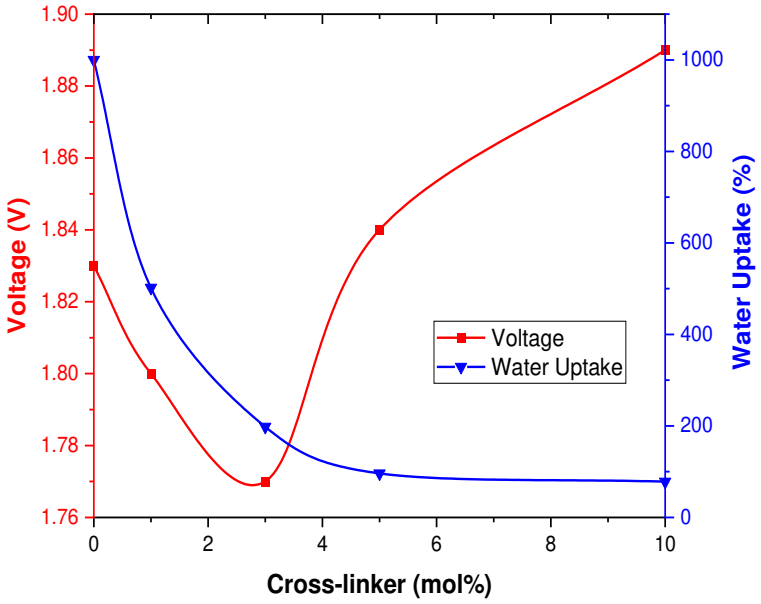

Figure 10. Cell voltage at 1 A/cm^2 (red) and water uptake (blue) vs. cross-linker concentration. The AEM was GT72 with PTFE reinforcement (30 μm thick, 10 mol% cross-linking). The anode ionomer was GT72-10 (25 wt%) and catalyst was $PbRuO_x$. The cathode catalyst was PtNi.

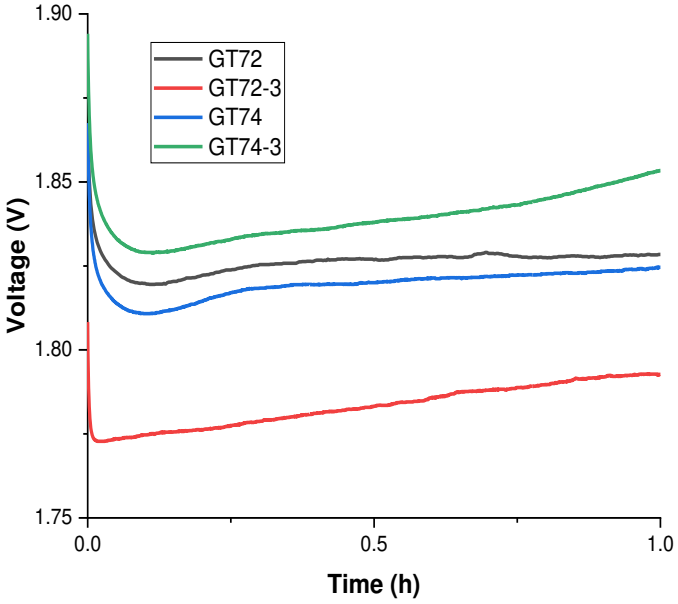

Figure 11. Cell voltage vs. time for MEAs with HER ionomers at 1 A/cm^2. The AEM was GT72 with PTFE reinforcement (30 μm thick, 10 mol% cross-linking). The anode ionomer was GT72-10 (25 wt%) and catalyst was $PbRuO_x$. The cathode catalyst was PtNi.

Discussion

The comparison between HER ionomers with high and low IEC, and the amount of cross-linking shows that performance is improved with ionic conductivity if excessive WU is avoided. There was a dramatic improvement in cell voltage (approximately 200 mV at 500 mA/cm^2 constant-current operation) when using high IEC ionomer compared to low IEC ionomer in the HER electrode. This result is contrary to previous observations for the OER ionomer where low IEC ionomers (with low conductivity and WU) outperformed high IEC ionomers in the absence of polymer cross-linking.[29] In the case of the OER electrode, WU was the critical factor in performance because excess swelling in the water-fed electrode negated the benefits of high ionic conductivity. Conductivity still played a role in cell performance, but it was a weak factor when there was high WU, especially in the flooded anode. The HER electrode, on the other hand, requires a higher local water activity because water is consumed at the HER electrode to form hydrogen and hydroxide ions, and is supplied only by diffusion from the water reservoir at the anode. The HER electrode is also a drier environment than the anode because it is not being supplied externally with liquid water. These results show that a more hydrophilic environment is needed at the HER electrode than at the OER electrode for optimal cell performance.

Figure 4 shows that cell performance was improved when the water content was changed by lowering the amount of high-IEC ionomer in the HER electrode. The volume fraction of water in the electrode (in the form of hydrated ionomer) decreases when the ionomer-to-catalyst ratio is decreased. The MEA with the lowest amount of ionomer (10%) showed the best performance among the four cells tested. Electrodes with <10% ionomer were not usable because of issues with catalyst detachment due to insufficient binder content. The MEA with the highest ionomer content (30%) showed the highest cell voltage and displayed performance stability issues after four hours

of constant current operation. These results show that although a higher water content is preferred at the HER, excess swelling in the HER electrode can be detrimental to both performance and stability.

The addition of a cross-linker to the ACI significantly lowered WU by limiting the swelling of the ionomer yet minimally affected the IEC and ionic conductivity. Restricting the swelling in the hydrated ionomer increased the density of quaternary ammonium head groups and facilitated more efficient ion conduction, compared to ionomers with a high degree of swelling. Figure 10 shows that the HER electrode was sensitive to the amount of cross-linker in the ionomer. This degree of sensitivity was not observed previously in an OER electrode.[29] This is because differences in ionomer swelling are less apparent in the fully flooded anode environment than in the drier cathode environment. The optimal amount of cross-linker was found to be 3 mol% TMHDA, which corresponds to a water uptake of 198%. A favorable cell performance of 1.77 V at 1 A/cm^2 was achieved using optimized HER and OER electrodes with a less conductive electrolyte (1 wt% vs. 3 wt% Na_2CO_3 in water), compared to the previous study.[29] This cell configuration is competitive with Nafion-based PEMELs and outperforms AEMELs built with other commercially available AEMs at higher operating temperature and NaOH electrolytes.[41, 42] Increasing or decreasing the amount of cross-linker in the HER ACI adversely affected the performance of the cell. The cell voltage rose by 30 to 60 mV when the HER ionomer cross-linker content was less than 3 mol% and WU was >500%. This behavior is similar to the flooded anode behavior observed previously when the ionomer content in the HER was increased. On the other hand, when the WU was decreased to <100% using a higher level of polymer cross-linker, the cell voltage rose by 70 to 120 mV. In this case, performance suffered more severely when there was a lower water content in the hydrogen evolving cathode due to low local water activity. It should

also be noted that GT72-10, which was previously found to be the best performing ionomer for the OER electrode, was the worst performing cross-linked ionomer for the HER electrode, among those compared.

Finally, the molecular weight of the ACI also had an impact on the effectiveness of the cross-linker. Non-cross-linked HER ionomers with comparable IEC performed similarly despite their differences in molecular weight. This observation was consistent with the previous report regarding non-cross-linked OER ionomers.[29] However, the shorter chain ionomer (GT74-3) did not show the same jump in performance as the longer chain ionomer (GT72-3) when the same amount of cross-linker was added. The performance of the MEA with GT74-3 was more similar to that of the non-cross-linked, higher molecular weight ionomer (GT72). This suggests that the molecular structure of cross-linked, higher molecular weight ionomers is more favorable for ion conduction. Chain entanglement within high molecular weight polymers may be responsible for the improved ion conduction.

The results from this study show that water management is needed in the HER electrode to a greater extent than in the OER electrode. These results also highlight the importance of using asymmetric ionomers that optimize the water content for the reactions at each electrolyzer electrode to achieve maximum cell performance.

Conclusions

Poly(norbornene) tetrablock copolymers with different ion exchange capacity were synthesized and used in the fabrication of hydrogen evolving electrodes in low-temperature AEM electrolyzers. It was found that ionomers with high IEC had better performance than ionomers with low IEC due to their higher ionic conductivity. The results also show that the HER electrode

requires an ionomer that maintains high water activity. Optimization of the ionomer-to-catalyst ratio in the cathode electrode showed that better performance and durability could be achieved by limiting the water content in cathode and by lowering the amount of ionomer present. Light cross-linking of the ionomer was used to manage the swelling of the ACI while maintaining high IEC and ionic conductivity. It was found that lowering the water uptake through cross-linking improved performance of the electrolyzer. Further reduction of the HER ionomer WU to below 200% had detrimental effects on cell performance. The highest achievable performance was 1.77 V at 1 A/cm^2 at 50 °C. The results of this study, as well as the results of the companion study on the OER ionomer, demonstrate the importance of managing water content in both AEM electrolyzer electrodes. These two studies also suggest the use of asymmetric ionomers to optimize the water content for the reactions at each electrode to achieve optimal cell performance.

Acknowledgements

The authors gratefully acknowledge the financial support of the U.S. Department of Energy, Office of Energy Efficiency & Renewable Energy H2@Scale program (Award Number: DE-EE0008833). The authors would also like to thank Pajarito Powder (Albuquerque, NM) for supplying electrocatalysts, Nel Hydrogen (Wallingford, CT) for supplying MEA materials and Xergy, Inc. (Harrington, DE) for fabrication of the composite membranes used in this study.

References

1. Zeng, K.; Zhang, D., Recent progress in alkaline water electrolysis for hydrogen production and applications. *Progress in Energy and Combustion Science* **2010,** *36* (3), 307-326.
2. Li, X.; Walsh, F. C.; Pletcher, D., Nickel based electrocatalysts for oxygen evolution in high current density, alkaline water electrolysers. *Physical Chemistry Chemical Physics* **2011,** *13* (3), 1162-1167.
3. Pérez-Alonso, F. J.; Adán, C.; Rojas, S.; Peña, M. A.; Fierro, J. L. G., Ni/Fe electrodes prepared by electrodeposition method over different substrates for oxygen evolution reaction in alkaline medium. *International Journal of Hydrogen Energy* **2014,** *39* (10), 5204-5212.
4. Shalom, M.; Ressnig, D.; Yang, X.; Clavel, G.; Fellinger, T. P.; Antonietti, M., Nickel nitride as an efficient electrocatalyst for water splitting. *Journal of Materials Chemistry A* **2015,** *3* (15), 8171-8177.
5. Herraiz-Cardona, I.; González-Buch, C.; Valero-Vidal, C.; Ortega, E.; Pérez-Herranz, V., Co-modification of Ni-based type Raney electrodeposits for hydrogen evolution reaction in alkaline media. *Journal of Power Sources* **2013,** *240*, 698-704.
6. Phillips, R.; Edwards, A.; Rome, B.; Jones, D. R.; Dunnill, C. W., Minimising the ohmic resistance of an alkaline electrolysis cell through effective cell design. *International Journal of Hydrogen Energy* **2017,** *42* (38), 23986-23994.
7. Pletcher, D.; Li, X.; Wang, S., A comparison of cathodes for zero gap alkaline water electrolysers for hydrogen production. *International Journal of Hydrogen Energy* **2012,** *37* (9), 7429-7435.
8. Kraglund, M. R.; Aili, D.; Jankova, K.; Christensen, E.; Li, Q.; Jensen, J. O., Zero-Gap Alkaline Water Electrolysis Using Ion-Solvating Polymer Electrolyte Membranes at Reduced KOH Concentrations. *Journal of The Electrochemical Society* **2016,** *163* (11), F3125-F3131.
9. Carmo, M.; Fritz, D. L.; Mergel, J.; Stolten, D., A comprehensive review on PEM water electrolysis. *International Journal of Hydrogen Energy* **2013,** *38* (12), 4901-4934.
10. Ursua, A.; Gandia, L. M.; Sanchis, P., Hydrogen Production From Water Electrolysis: Current Status and Future Trends. *Proceedings of the IEEE* **2012,** *100* (2), 410-426.
11. Millet, P.; Mbemba, N.; Grigoriev, S. A.; Fateev, V. N.; Aukauloo, A.; Etiévant, C., Electrochemical performances of PEM water electrolysis cells and perspectives. *International Journal of Hydrogen Energy* **2011,** *36* (6), 4134-4142.
12. Babic, U.; Suermann, M.; Büchi, F. N.; Gubler, L.; Schmidt, T. J., Critical Review—Identifying Critical Gaps for Polymer Electrolyte Water Electrolysis Development. *Journal of The Electrochemical Society* **2017,** *164* (4), F387-F399.
13. Li, H.; Inada, A.; Fujigaya, T.; Nakajima, H.; Sasaki, K.; Ito, K., Effects of operating conditions on performance of high-temperature polymer electrolyte water electrolyzer. *Journal of Power Sources* **2016,** *318*, 192-199.
14. Li, D.; Park, E. J.; Zhu, W.; Shi, Q.; Zhou, Y.; Tian, H.; Lin, Y.; Serov, A.; Zulevi, B.; Baca, E. D.; Fujimoto, C.; Chung, H. T.; Kim, Y. S., Highly quaternized polystyrene ionomers for high performance anion exchange membrane water electrolysers. *Nature Energy* **2020**.
15. Barbir, F., PEM electrolysis for production of hydrogen from renewable energy sources. *Solar Energy* **2005,** *78* (5), 661-669.

16. Buttler, A.; Spliethoff, H., Current status of water electrolysis for energy storage, grid balancing and sector coupling via power-to-gas and power-to-liquids: A review. *Renewable and Sustainable Energy Reviews* **2018,** *82*, 2440-2454.
17. Pavel, C. C.; Cecconi, F.; Emiliani, C.; Santiccioli, S.; Scaffidi, A.; Catanorchi, S.; Comotti, M., Highly Efficient Platinum Group Metal Free Based Membrane-Electrode Assembly for Anion Exchange Membrane Water Electrolysis. *Angewandte Chemie International Edition* **2014,** *53* (5), 1378-1381.
18. Bessarabov, D.; Millet, P.; Pollet, B. G., *PEM Water Electrolysis*. Elsevier Science: 2018.
19. Vincent, I.; Kruger, A.; Bessarabov, D., Hydrogen Production by water Electrolysis with an Ultrathin Anion-exchange membrane (AEM). *International Journal of Electrochemical Science* **2018,** *13*, 11347-11358.
20. Mandal, M.; Huang, G.; Kohl, P. A., Anionic multiblock copolymer membrane based on vinyl addition polymerization of norbornenes: Applications in anion-exchange membrane fuel cells. *Journal of Membrane Science* **2019,** *570-571*, 394-402.
21. Mandal, M.; Huang, G.; Kohl, P. A., Highly Conductive Anion-Exchange Membranes Based on Cross-Linked Poly(norbornene): Vinyl Addition Polymerization. *ACS Applied Energy Materials* **2019,** *2* (4), 2447-2457.
22. Chen, W.; Mandal, M.; Huang, G.; Wu, X.; He, G.; Kohl, P. A., Highly Conducting Anion-Exchange Membranes Based on Cross-Linked Poly(norbornene): Ring Opening Metathesis Polymerization. *ACS Applied Energy Materials* **2019,** *2* (4), 2458-2468.
23. Huang, G.; Mandal, M.; Peng, X.; Yang-Neyerlin, A. C.; Pivovar, B. S.; Mustain, W. E.; Kohl, P. A., Composite Poly(norbornene) Anion Conducting Membranes for Achieving Durability, Water Management and High Power (3.4 W/cm2) in Hydrogen/Oxygen Alkaline Fuel Cells. *Journal of The Electrochemical Society* **2019,** *166* (10), F637-F644.
24. Mandal, M.; Huang, G.; Hassan, N. U.; Peng, X.; Gu, T.; Brooks-Starks, A. H.; Bahar, B.; Mustain, W. E.; Kohl, P. A., The Importance of Water Transport in High Conductivity and High-Power Alkaline Fuel Cells. *Journal of The Electrochemical Society* **2019,** *167* (5), 054501.
25. Varcoe, J. R.; Atanassov, P.; Dekel, D. R.; Herring, A. M.; Hickner, M. A.; Kohl, P. A.; Kucernak, A. R.; Mustain, W. E.; Nijmeijer, K.; Scott, K.; Xu, T.; Zhuang, L., Anion-exchange membranes in electrochemical energy systems. *Energy & Environmental Science* **2014,** *7* (10), 3135-3191.
26. Wang, L.; Bellini, M.; Miller, H. A.; Varcoe, J. R., A high conductivity ultrathin anion-exchange membrane with 500+ h alkali stability for use in alkaline membrane fuel cells that can achieve 2 W cm−2 at 80 °C. *Journal of Materials Chemistry A* **2018,** *6* (31), 15404-15412.
27. Mandal, M.; Huang, G.; Hassan, N. U.; Mustain, W. E.; Kohl, P. A., Poly(norbornene) anion conductive membranes: homopolymer, block copolymer and random copolymer properties and performance. *Journal of Materials Chemistry A* **2020,** *8* (34), 17568-17578.
28. Ul Hassan, N.; Mandal, M.; Huang, G.; Firouzjaie, H. A.; Kohl, P. A.; Mustain, W. E., Achieving High-Performance and 2000 h Stability in Anion Exchange Membrane Fuel Cells by Manipulating Ionomer Properties and Electrode Optimization. *Advanced Energy Materials* **2020**, 2001986.
29. Huang, G.; Mandal, M.; Hassan, N. U.; Groenhout, K.; Dobbs, A.; Mustain, W. E.; Kohl, P. A., Ionomer Optimization for Water Uptake and Swelling in Anion Exchange

Membrane Electrolyzer: Oxygen Evolution Electrode. *Journal of the Electrochemical Society* **2020,** *167* (16), 164514.
30. Ahlfield, J.; Huang, G.; Liu, L.; Kaburagi, Y.; Kim, Y.; Kohl, P. A., Anion Conducting Ionomers for Fuel Cells and Electrolyzers. *Journal of The Electrochemical Society* **2017,** *164* (14), F1648-F1653.
31. Wang, Z.; Mandal, M.; Sankarasubramanian, S.; Huang, G.; Kohl, P. A.; Ramani, V. K., Influence of Water Transport Across Microscale Bipolar Interfaces on the Performance of Direct Borohydride Fuel Cells. *ACS Applied Energy Materials* **2020,** *3* (5), 4449-4456.
32. Gu, S.; Cai, R.; Luo, T.; Chen, Z.; Sun, M.; Liu, Y.; He, G.; Yan, Y., A Soluble and Highly Conductive Ionomer for High-Performance Hydroxide Exchange Membrane Fuel Cells. *Angewandte Chemie International Edition* **2009,** *48* (35), 6499-6502.
33. Zhang, D.; Zeng, K., Evaluating the Behavior of Electrolytic Gas Bubbles and Their Effect on the Cell Voltage in Alkaline Water Electrolysis. *Industrial & Engineering Chemistry Research* **2012,** *51* (42), 13825-13832.
34. Omasta, T. J.; Wang, L.; Peng, X.; Lewis, C. A.; Varcoe, J. R.; Mustain, W. E., Importance of balancing membrane and electrode water in anion exchange membrane fuel cells. *Journal of Power Sources* **2018,** *375*, 205-213.
35. Omasta, T. J.; Park, A. M.; LaManna, J. M.; Zhang, Y.; Peng, X.; Wang, L.; Jacobson, D. L.; Varcoe, J. R.; Hussey, D. S.; Pivovar, B. S.; Mustain, W. E., Beyond catalysis and membranes: visualizing and solving the challenge of electrode water accumulation and flooding in AEMFCs. *Energy & Environmental Science* **2018,** *11* (3), 551-558.
36. Zheng, Y.; Huang, G.; Wang, L.; Varcoe, J. R.; Kohl, P. A.; Mustain, W. E., Effect of reacting gas flowrates and hydration on the carbonation of anion exchange membrane fuel cells in the presence of CO2. *Journal of Power Sources* **2020,** *467*, 228350.
37. Dekel, D. R., Review of cell performance in anion exchange membrane fuel cells. *Journal of Power Sources* **2018,** *375*, 158-169.
38. Dekel, D. R.; Rasin, I. G.; Page, M.; Brandon, S., Steady state and transient simulation of anion exchange membrane fuel cells. *Journal of Power Sources* **2018,** *375*, 191-204.
39. Yang, D.; Yu, H.; Li, G.; Zhao, Y.; Liu, Y.; Zhang, C.; Song, W.; Shao, Z., Fine microstructure of high performance electrode in alkaline anion exchange membrane fuel cells. *Journal of Power Sources* **2014,** *267*, 39-47.
40. Liu, L.; Huang, G.; Kohl, P. A., Anion conducting multiblock copolymers with multiple head-groups. *Journal of Materials Chemistry A* **2018,** *6* (19), 9000-9008.
41. Henkensmeier, D.; Najibah, M.; Harms, C.; Žitka, J.; Hnát, J.; Bouzek, K., Overview: State-of-the Art Commercial Membranes for Anion Exchange Membrane Water Electrolysis. *Journal of Electrochemical Energy Conversion and Storage* **2020,** *18* (2).
42. Bender, G.; Carmo, M.; Smolinka, T.; Gago, A.; Danilovic, N.; Mueller, M.; Ganci, F.; Fallisch, A.; Lettenmeier, P.; Friedrich, K. A.; Ayers, K.; Pivovar, B.; Mergel, J.; Stolten, D., Initial approaches in benchmarking and round robin testing for proton exchange membrane water electrolyzers. *International Journal of Hydrogen Energy* **2019,** *44* (18), 9174-9187.